THE ASTROPHYSICAL JOURNAL, 283:566–572, 1984 August 15

FAR-INFRARED AND SUBMILLIMETER SURVEY OF THE GALACTIC PLANE FROM $l = 11^\circ\!.5$ TO $l = 17^\circ\!.5$

M. F. CAMPBELL,[1] R. F. SILVERBERG,[2] W. F. HOFFMANN,[3] M. G. HAUSER,[2] D. W. NILES,[1]
M. T. STIER,[2] H. A. THRONSON, JR.,[3,4] AND T. KELSALL[2]
Received 1983 October 20; accepted 1984 February 29

ABSTRACT

Medium resolution (11′) maps of the galactic plane are presented from $l = 11^\circ\!.5$ to $l = 17^\circ\!.5$ at wavelengths of 93 μm, 154 μm, and 190 μm. The maps are interpreted in terms of the temperature and spatial structure of diffuse far-infrared/submillimeter sources associated with evolved H II regions and a continuous ridge of galactic emission. The emission regions are found to be more extended at the longer wavelengths which implies that there must be a range of dust temperatures in the sources. The properties of the galactic ridge are similar to those of the sources.

Subject headings: galaxies: Milky Way — infrared: sources — nebulae: H II regions

I. INTRODUCTION

Large-scale surveys of far-infrared and submillimeter emission from the galactic plane can be used to address questions related to the large-scale distribution of gas and luminous stars in the Galaxy in addition to those related to the structure of individual extended infrared sources. A major question exists as to whether the interstellar dust which emits diffuse far-infrared and submillimeter radiation is more strongly associated with molecular clouds observed primarily in CO radio emission lines or with ionized gas observed in radio continuum. Recent observational data of large-scale infrared surveys have been reviewed by Okuda (1981), and the interpretation was reviewed by Drapatz (1981). Most infrared surveys of the galactic plane have utilized beams $\gtrsim 30'$ (Okuda); however, a high-resolution (1′) survey has been made from $l \sim 12^\circ$ to $l \sim 16^\circ$ by Jaffe, Stier, and Fazio (1982, hereafter JSF). We present far-infrared and submillimeter maps made with $\sim 11'$ beams of the galactic plane covering longitudes from $11^\circ\!.5$ to $17^\circ\!.5$. The maps were obtained as parts of surveys of the Galaxy with the Steward Observatory (SO) cryogenically-cooled far-infrared survey telescope and the Goddard Space Flight Center (GSFC) submillimeter survey telescope, both of which were flown on high-altitude balloons from the National Scientific Balloon Facility in Palestine, Texas. These maps provide higher spatial resolution than previous high-sensitivity surveys of diffuse galactic emission at several wavelengths which define the peak in the spectrum. The present region of study was chosen partly because a comparison with the 1′ JSF survey could be made.

II. OBSERVATIONS

a) Steward Observatory Data

The map shown in Figure 1 was obtained by the SO telescope. The telescope and data reduction for it have been discussed by Campbell (1979) and Campbell *et al.* (1980, 1981). The filter's half-power points were 73 μm and 113 μm, determined from laboratory measurements. The data were obtained by scanning in cross elevation with a 10° scan length, producing a track which intersected the galactic equator at an angle of 74°. The beamwidth perpendicular to the scanning direction was 11′ (FWHM); the chopper throw was 18′ in cross elevation. Restoration of the data to provide the map required the application of a spatial filter which effectively broadened the beam to 17′ in cross elevation. The source at G13.2+0.0 shows the effects of the beam asymmetry and the scan direction. Positional information was determined from sightings of visible stars with an auxiliary photometer giving an rms uncertainty of 3′ in each coordinate.

At the time of the SO balloon flight in 1979 August, no planet was available for calibration. M17 was chosen to be the calibration object, and the data of Hoffmann, Frederick, and Emery (1971) were used. Their 100 μm peak brightness, which was uncorrected for diffuse emission, was scaled to the effective wavelength of the present filter of 85 μm using the 75 K graybody spectrum given by Ward, Gull, and Harwit (1977), and the result was used to calibrate the chopped peak brightness of M17 in the new data. This calibration gives 3.3×10^3 Jy per beam for Figure 1. The spatial filter used in preparing the map reduces peak brightnesses somewhat, with the amount dependent on an individual source's extension, but it has no effect on the total spatially integrated flux densities, which are presented in Table 1. Our data are in reasonably good agreement with large-beam measurements of M17 by Olthof (1974), Nishimura, Low, and Kurtz (1980), and Gispert, Puget, and Serra (1982), falling between the fluxes presented by the latter two papers. In addition, we have compared our integrated flux density for M17 of 8.6×10^5 Jy at 85 μm to that of the map by Wilson *et al.* (1979), which was made at higher spatial resolution and with a long pass filter for which they calculated a flux density of 6.6×10^5 Jy at an effective wavelength of 69 μm. Correcting for the different effective wavelengths makes the discrepancy about 10% larger, but when scans through their map were convolved with our beam and compared with our data, it was found that their telescope with a 1′ beam and a 5′ chopper throw had missed some diffuse emission, and that a diffuse component of the emission can account for the discrepancy.

Combining the SO and GSFC data (see below) shows that sources other than M17 are appreciably cooler with a typical

[1] Department of Physics and Astronomy, Colby College.
[2] NASA/Goddard Space Flight Center.
[3] Steward Observatory, University of Arizona.
[4] Department of Physics and Astronomy, University of Wyoming.

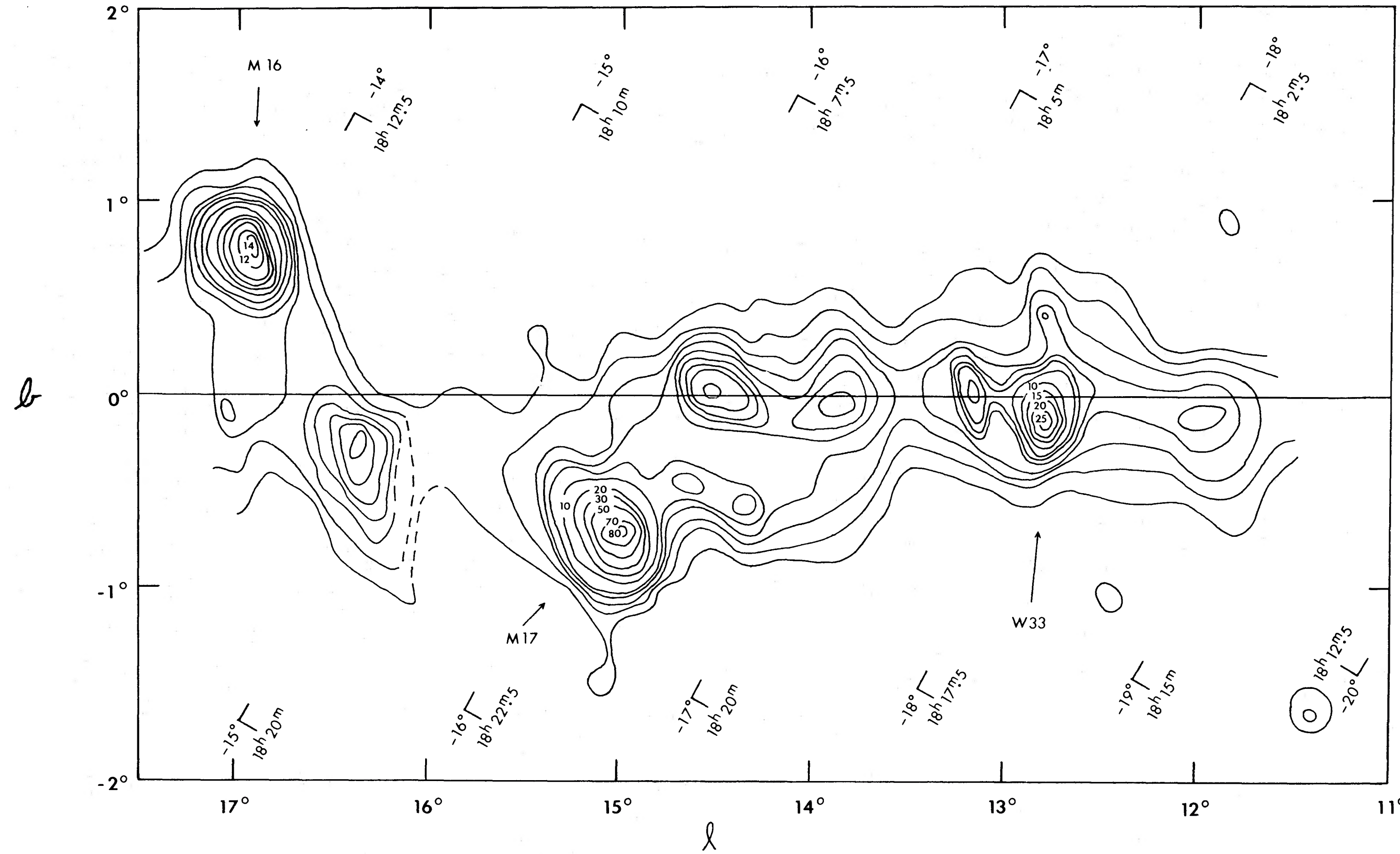

FIG. 1.—Map of far-infrared flux density in the 73–113 μm filter of the SO telescope. For a typical source with a 25 K, $\epsilon \propto \lambda^{-1}$ spectrum, each contour represents 3.9×10^3 Jy per beam. The calibration is discussed in the text. The noise level is about one-third contour.

TABLE 1

FAR-INRARED AND SUBMILLIMETER SOURCE PROPERTIES

Source (1)	G (93 μm) (2)	Total Flux Density at 93 μm[a] (Jy) (3)	Source FWHM[b] (93 μm) (4)	Galactic Ridge FWHM[b] (5)	G (154 μm) (6)	Total Flux Density at 154 μm[a] (Jy) (7)	Source FWHM (154 μm)[b] (8)	Galactic Ridge FWHM[b] (9)	Total Flux Density at 190 μm[a] (Jy) (10)	*T* (K) (11)
1(W33)	12.8−0.2	3.0×10^5	U[c]	22	12.8−0.1	3.9×10^5	U[c]	39	2.5×10^5	28
2	13.2+0.0	1.3×10^5	11	43	13.2+0.0	3.2×10^5	28	57	2.1×10^5	23
3	13.9−0.1	3.3×10^5	19	59	13.9+0.0	5.5×10^5	42	81	3.6×10^5	25
4	14.6+0.1	2.6×10^5	13	54	14.5+0.0	3.5×10^5	18	87	2.1×10^5	27
5(M17)	15.0−0.7	8.2×10^5	5	...	15.0−0.6	6.2×10^5	11	...	3.7×10^5	37
6	16.4−0.3	2.4×10^5	15	41	16.4−0.2	6.3×10^5	25	92	4.2×10^5	22
7(M16)	16.9+0.8	3.6×10^5	15	68	17.0+0.9	3.9×10^5	28	99	2.4×10^5	30

[a] Not corrected for galactic ridge component.
[b] Corrected for beam.
[c] Unresolved.

dust temperature of 25 K. The SO flux densities have been calculated using a dust temperature of 25 K and an emissivity proportional to λ^{-1} over the SO filter. The emissivity law is characteristic of far-infrared sources associated with H II regions (e.g., Thronson and Harper 1979). Sources of this temperature and emissivity give an effective wavelength of 93 μm and an effective bandwidth of 1.2×10^{12} Hz in the SO filter. The calibration for regions other than M17 in Figure 1 is therefore 3.9×10^3 Jy per beam per contour at 93 μm. Because of the indirect nature of the calibration, its uncertainty is estimated to be 40%.

b) Goddard Space Flight Center Data

The maps shown in Figure 2 and Figure 3 were obtained by the GSFC telescope in 1980 August. This telescope and its use have been described by Silverberg *et al.* (1980). It utilizes a 11.′5 beam with a 20′ chopper throw. Scans were in cross elevation at approximately 70° to the galactic equator. Low pass filters were used which have effective wavelengths of 154 μm and 190 μm and bandwidths of 1.2×10^{12} Hz and 9.1×10^{11} Hz in response to a 25 K spectrum which has been modified by an emissivity proportional to λ^{-2} for $\lambda > 150$ μm and proportional to λ^{-1} for $\lambda < 150$ μm. This emissivity law combines the observational evidence at relatively short wavelengths cited above with that at longer wavelengths (e.g., Keene 1981; Schwartz 1982). The location of the break in slope is somewhat arbitrary; if a strict λ^{-2} law is assumed at all wavelengths, the 190 μm effective wavelength is negligibly changed, and the bandwidth for the 154 μm channel is reduced only 10%. The calibration for Figure 2 is 6.2×10^3 Jy per beam per contour and 6.0×10^3 Jy per beam per contour for Figure 3.

Since no planets were available during the 1980 GSFC flight, the calibration for the 154 μm channel was transferred via M17 from the 1979 flight of the GSFC telescope when both Jupiter and M17 were observed. The 190 μm channel was not in the photometer during the 1979 flight, hence its calibration is less direct. The 154 to 190 μm channel flux ratio was calculated assuming M17 to be a 33 K object with a λ^{-2} emissivity, consistent with observations on the 1979 flight. The 190 μm channel flux calibration was scaled from the 154 μm channel. Data were also obtained in a channel of 310 μm effective wavelength but at a much lower signal-to-noise ratio; these data have not been included in this analysis.

Experience with both telescopes has shown that repro-

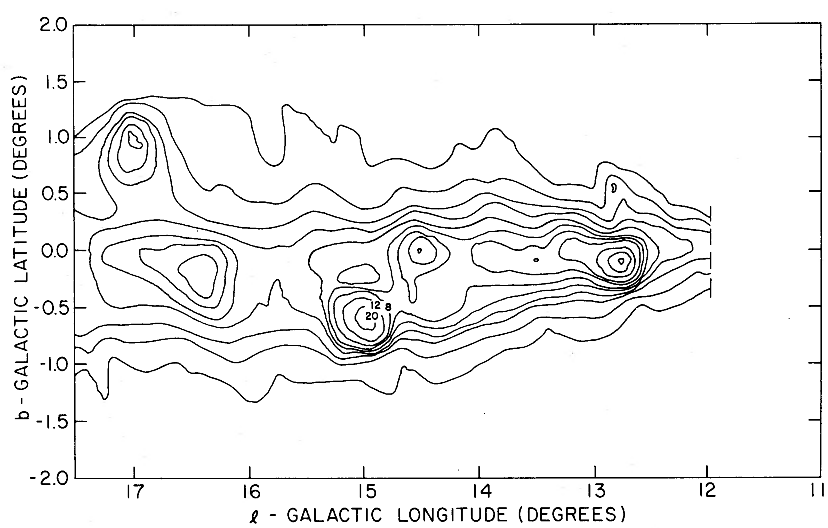

FIG. 2.—Map of submillimeter flux density obtained by the GSFC telescope at an effective wavelength of 154 μm (assuming 25 K dust with $\epsilon \propto \lambda^{-2}$ for $\lambda > 150$ μm and $\epsilon \propto \lambda^{-1}$ for $\lambda < 150$ μm). Each contour represents 6.2×10^3 Jy per 11.′5 beam. The calibration is discussed in the text. Scans intersected the galactic plane at approximately 70°, and the boundary of the area scanned is shown. The noise level is about one-third contour.

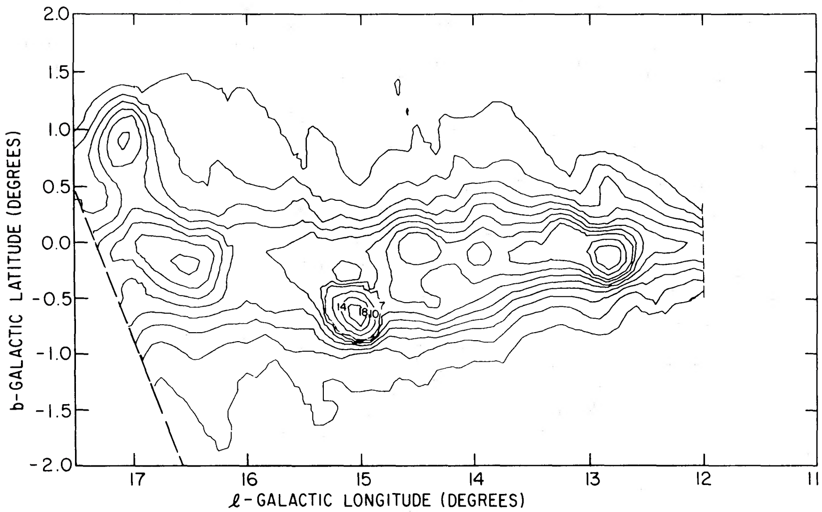

FIG. 3.—Map of submillimeter flux density obtained by GSFC telescope at an effective wavelength of 190 μm for a spectrum as in Fig. 2. Each contour represents 4.0×10^3 Jy per beam. The noise level is about one-fifth contour.

ducibility in peak brightness for sources which are rescanned is better than 30%.

c) *Derivation of Temperatures and Source Widths*

The seven brightest peaks in Figure 1 were selected for analysis as discrete, though extended, sources. They are listed in Table 1. For each, the galactic coordinate (G number) is given for the 93 μm peak from the SO map and for the 154 μm peak of the GSFC map. Total flux densities derived by spatially integrating the maps over areas chosen to contain the entire emission associated with the peaks are presented in Table 1. This procedure makes correction for different beam sizes unnecessary. However, there has been no correction for the underlying emission due to the more extended galactic ridge. The flux densities were fitted to a single-temperature dust model using an emissivity law which changes from $\epsilon \propto \lambda^{-1}$ (at short wavelengths) to $\epsilon \propto \lambda^{-2}$ at 150 μm. Changing the location of the break in the assumed emissivity law by ± 20 μm has only a 1 K effect on the derived temperature. Figure 4 shows that this emissivity law with a temperature of 25 K fits the data for source 3, as an example, rather well. Other sources can be fitted as well as the fit shown for source 3. The single-component dust model temperatures are shown in the last column of Table 1.

The effect of assuming an emissivity law proportional to λ^{-2} at all wavelengths was also investigated. The typical source temperature (excluding M17) for this emissivity law would be 22 K. (A 20 K, $\epsilon \propto \lambda^{-2}$ spectrum changes both effective wavelengths and filter widths by less than 8% at 93 μm and has an even smaller effect on the GSFC data.) Spectra with a single emissivity law generally fit the data about as well as those with the break near 150 μm.

Gaussian profiles have been fitted to cuts through the peaks of each source perpendicular to the galactic plane for the 93 μm and 154 μm maps. In every case, two Gaussians are required to obtain a good fit—one for the source and one for the much broader component attributed to the galactic ridge. Both widths are listed in Table 1. Figure 5 shows the components for source 3.

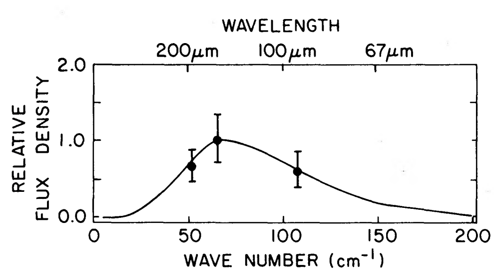

FIG. 4

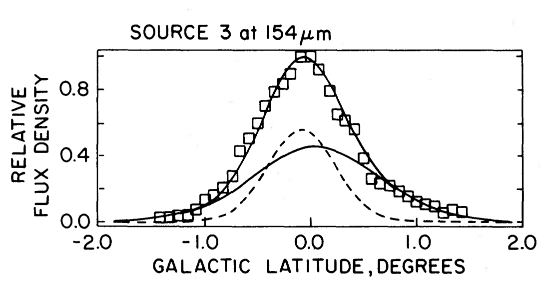

FIG. 5

FIG. 4.—Relative spectral points for source 3 (G 13.9−0.1) compared to a 25 K spectrum with $\epsilon \propto \lambda^{-2}$ for $\lambda \geq 150$ μm and $\epsilon \propto \lambda^{-1}$ for $\lambda \leq 150$ μm. The error bars represent the uncertainty of the calibration rather than statistical errors.

FIG. 5.—Gaussian curves fitted to the measured brightness profiles (*squares*) of source 3 (G13.9−0.1) from Fig. 1 (93 μm) and Fig. 2 (154 μm). In each profile two Gaussians are fitted: one to the discrete source and one to the galactic ridge. The sum of the two is also shown. The widths of the fitted Gaussians are shown in Table 1, after correction for the telescope beam size.

III. DISCUSSION

a) Temperatures in the Sources and the Diffuse Galactic Ridge

The profiles of intensity parallel to galactic latitude for the sources indicate that each source has a broad underlying component which we have identified with diffuse emission from the galactic plane (see, e.g., Fig. 5). Although we have not attempted to fit curves through the peaks in the longitudinal direction, it seems clear from the maps that the diffuse component is indeed a ridge which persists even in regions where no compact source exists. The width of the broad component is variable at 93 μm and may be affected by the individual sources. At the longer wavelengths, the ridge width shows much less influence of the individual sources although it appears to increase in width with increasing galactic longitude in this longitude range. The approximately uniform character of the ridge at submillimeter wavelengths and the much less uniform character at 93 μm persists elsewhere in the galactic plane where we have surveyed.

The best example of the ridge far from sources is at $l \approx 15\overset{\circ}{.}7$. At 154 μm, the width of the ridge there is $\sim 80'$, which is only slightly smaller than the values shown for the ridge at the adjacent sources. Because of the high density of sources and their complex profiles in two dimensions, we have not attempted to remove them from the ridge to present a map of the diffuse component alone. However, we have estimated the flux densities due to the compact components alone, and we find that the ridge contributes about 1.8×10^6 Jy of the total of 3.3×10^6 Jy represented within the lowest contour of the map in Figure 1, with the compact source contribution dominated by M17.

The sources and galactic ridge are much more extended at longer wavelengths than at 93 μm. The ratio of source width at 165 μm to source width at 93 μm is approximately the same for all discrete sources and for the ridge, indicating similar thermal and density structures. Typical ratios of peak brightnesses at the two wavelengths are very similar for both source and ridge components, also indicating similar temperatures. The width of the galactic ridge component at 154 μm is consistent with that given by Nishimura, Low, and Kutz (1980), whose observations were made without chopping.

Because the sources and galactic ridge are more extended at 154 μm that at 93 μm (except for sources 1 and 5), it is not correct to interpret temperatures from Table 1 as physical temperatures. As an example, consider source 3. Its spectrum may be adequately fitted by a single 25 K spectrum with a dust emissivity law as described above (Fig. 3). However, the different spatial widths observed at 93 and 154 μm imply that more than one temperature component is contributing to the observed emission. With the limited spectral coverage and data quality we have, more detailed modeling is not warranted.

Apparent temperatures were also estimated for the central portions of the resolved sources. These temperatures were typically 2–5 K hotter than the average apparent temperatures calculated using the total flux densities over the source, but are less certain because of differences in the beam sizes of the SO and GSFC instruments. This suggests a temperature structure as might be expected for a centrally heated source. We also note that the apparent temperatures cited here for the sources are significantly lower than those obtained using smaller beams (Harvey, Campbell, and Hoffmann 1977; Thronson and Harper 1979). This may be due to beam size effects as suggested by Scoville and Kwan (1976).

The galactic ridge has an apparent temperature similar to that of the individual sources. Its emission is therefore consistent with dust having a similar temperature distribution. This apparent temperature is significantly hotter than the 18 K estimated for the ridge by Nishimura, Low, and Kurtz (1980) using $\epsilon \propto \lambda^{-1.5}$ for their measurements with a 30′ beam. Since the ridge is broader than the sources but has the same apparent temperature, one might suspect that the heating radiation is similar to that in the compact sources, though it may come from spatially distributed unresolved centers.

b) Morphological Comparisons with Radio Continuum and CO Surveys

Comparisons of our survey with ones of similar resolution in radio continuum and ^{12}CO line emission show several interesting effects. When the 93 μm map is compared to the 11′ beam radio continuum survey of Altenhoff *et al.* (1970), a one-to-one association is found between our sources and bright thermal radio sources, although there are some positional offsets which can be attributed to our positional uncertainty. It is not as easy to make such associations by comparing the far-infrared to a map of ^{12}CO emission summed over all velocites from the GISS/Columbia University CO survey (Thaddeus 1982). When comparison is made with maps summed over limited velocity ranges, however, associations between the far-infrared sources and molecular clouds are more easily made. Sources 1, 2, 3, 4, and 6 appear to be associated with clouds in the range $35 \leq V_{\rm LSR} \leq 55$ km s^{-1}, and sources 5 and 7 (M17 and M16) with clouds in $11 \leq V_{\rm LSR} \leq 30$ km s^{-1}. The two weak 93 μm sources near M17 at $l = 14\overset{\circ}{.}4$ and $14\overset{\circ}{.}6$ and the weak source near W33 at $l = 12\overset{\circ}{.}8$, $b = 0\overset{\circ}{.}43$ may be associated with CO in the 11–30 km s^{-1} range, which Elmegreen, Lada, and Dickenson (1979) attribute to the M17 giant molecular cloud. There are molecular clouds in each range which are *not* associated with far-infrared sources, particularly for the velocity range of 11–30 km s^{-1}.

The spatial association of far-infrared and radio continuum emission emphasizes that a strong infrared source is found only when a stellar heating source is present; high dust density alone is not sufficient. Indeed, *high* dust density may not be necessary for infrared emission since a visual extinction of only a few magnitudes will convert all stellar radiation into the infrared. Our large beams can sample long path lengths across relatively low density sources, which, despite their low densities, are optically thick to visible radiation and are diffuse infrared sources. This is not to say that the submillimeter emission originates from inside extended H II regions; the sizes of the 154 μm sources in Table 1 are significantly larger than the associated sources in the 11′ survey of radio continuum of Altenhoff *et al.* (1970), although the 93 μm and radio continuum sizes are similar.

It is interesting to note that the velocity range $35 \leq V_{\rm LSR} \leq 55$ km s^{-1} places sources 1, 2, 3, 4, and 6 at near-kinematic distances of about 5 kpc (see Stier *et al.* 1982 and § III*d* below), and they could be associated with the "5 kpc" molecular ring. A significant fraction of extended CO emission also comes in the 35–55 km s^{-1} range. If the far-infrared and CO emission come from the same physical regions, then the $\sim 1°$ FWHM observed in the far-infrared for the ridge component corresponds to a scale height of ~ 90 pc. This is typical of the scale height of O and B stars in the Galaxy (Allen 1973) and CO (Gordon and Burton 1976).

c) *Comparison with a High Spatial Resolution Far-Infrared Survey*

We now turn to a comparison of our survey with the 1′ survey of the Harvard-Smithsonian balloon-borne far-infrared telescope (JSF) which uses a broad-band filter at an effective wavelength of 69 μm. Sources in the JSF survey cover the same range in galactic latitude as our maps, and there is a general association of the stronger JSF sources with our seven sources, or other features in the 93 μm map. Typically each of our sources encompasses three to six JSF sources.

We choose to compare bolometric fluxes and proceed in the following way: for each source in Table 1, an approximate fraction of flux to subtract for the contribution due to the galactic ridge is calculated. This correction is negligible for M16 and M17, and is about 70% for sources 2, 3, 4, and 6. The spectrum indicated by our assumed emissivity law, the 93 μm flux density, and the temperature shown in Table 1 are then used to find the source flux in W m^{-2}. All of the JSF sources in the area spatially integrated for each large beam source have their fluxes calculated from the luminosities and distances quoted in JSF. This procedure minimizes the difficulties in comparing two sets of measurements which do not cover exactly the same spectral range. The SO and GSFC data can be viewed as equivalent to data from a long pass filter whose cut-on is at 80 μm, while the JSF data were taken with a long pass filter which cuts on at 40 μm. Estimation of the bolometric flux from either the present data or the JSF data is insensitive to the assumed spectrum for the typical cold source temperatures, with results varying by less than 20% for spectra with $\epsilon \propto \lambda^{-1}$ or $\epsilon \propto \lambda^{-2}$ and temperatures within the range shown in Table 1.

We get reasonable agreement with the high-resolution data for the fluxes for M17 (using the data quoted by Wilson *et al.* 1979 rather than by JSF) and for W33, within the uncertainties of the absolute calibrations. For the remaining sources common to both surveys (2, 3, and 4), the large beam telescopes observe about 4 times the flux reported by JSF. For M16 we observe about 3 times the flux reported by McBreen, Fazio, and Jaffe (1982). The larger fluxes presented here may be largely due to diffuse emission associated with evolved H II regions which the Harvard-Smithsonian telescope could not detect with its smaller chopper throw and much smaller beam. It would appear that in evolved H II regions, far-infrared emission originates *both* from high-density molecular cloud fragments and from more diffuse parts of the region. M17 and W33 have their emission dominated by the high-density regions, whereas for the others the emission is dominated by the diffuse regions. McBreen, Fazio, and Jaffe commented that M16 is severely density bounded. If the diffuse flux reported here is included, $1.4 \times 10^6\ L_\odot$ of the estimated $2.2 \times 10^6\ L_\odot$ of the exciting star is accounted for in the far-infrared.

While the small-beam survey did not detect major diffuse emission due to the sources and due to the galactic ridge, it does appear to have detected the major centers of excitation for the sources observed in our large-beam observations. No sources were found in the large-beam surveys which lacked small-scale high surface brightness components observed by JSF.

d) *Comparison of Luminosities Derived from Radio Continuum and Far-Infrared Observations*

For H II regions whose small-scale structure and distances are well known, it is useful to compare the luminosities derived from the far-infrared to those of the exciting star or stars as deduced from the radio continuum flux, using stellar models such as those of Panagia (1973). Although the large-beam radio sources are certainly composed of smaller scale structures (Altenhoff *et al.* 1978), it is still useful to apply such an analysis under the assumption of simple geometry. The result of the analysis is shown in Table 2. Column (1) identifies the source as in Table 1. Column (2) shows an estimate of the 93 μm flux densities after subtraction of the diffuse galactic ridge component. This background subtraction is accomplished by assuming the source is a two-dimensional Gaussian and the ridge is a one-dimensional Gaussian with each component of the width and magnitude determined by fitting a slice (see Fig. 5).

Column (3) in Table 2 shows assumed distances. These are taken to be consistent with the work of the Harvard-Smithsonian group (JSF; Wilson *et al.* 1979; McBreen, Fazio, and Jaffe 1982). In most cases, all of the JSF sources we associate with a single source in Table 2 are assigned the same or nearly the same kinematic distance by JSF and Stier *et al.* (1982). We have taken a distance consistent with the strongest JSF sources where there is a large range in distance. It is worth noting that H109α and CO line velocities are generally consistent for these sources (see Stier *et al.*). The sources' luminosities (col. [4]) are then calculated using bolometric fluxes whose derivation was described above. We estimate that the luminosities derived in this way are correct within a factor of ~ 3 assuming the distances used are correct.

Radio data were taken from the survey of Altenhoff *et al.* (1970) because of the similarity in beam sizes. These data are shown in columns (6) and (7). Although there is a lack of detailed morphological agreement between 93 μm and 5 GHz maps for the sources, their sizes are similar at these two wavelengths. The number of ionizing photons, N_L, is calculated using Rubin's (1968) approximate equation for optically thin

TABLE 2

DERIVED LUMINOSITIES

Source (1)	F_ν (93 μm) (Compact) (Jy) (2)	Assumed Distance (kpc) (3)	$L_{IR}/L_\odot$ (4)	Radio ID (5)	F_ν (5.0 GHz) (Jy) (6)	N_L (s^{-1}) (7)	$L/L_\odot$ (ZAMS) (8)
1(W33)	7.2×10^4	3.8	1.2×10^6	G 12.8−0.2	39	5.9×10^{49}	9.2×10^5
2	5.5×10^4	4.7	1.7×10^6	G 13.2+0.0	6	1.4×10^{49}	2.8×10^5
3	6.9×10^4	4.0	1.4×10^6	G 14.2−0.2	26	4.3×10^{49}	6.9×10^5
4	9.1×10^4	3.8	1.6×10^6	G 14.6+0.1	30	4.5×10^{49}	7.2×10^5
5(M17)	8.2×10^5	2.1	7.2×10^6	G 15.1−0.7	554	2.5×10^{50}	3.4×10^6
6	5.8×10^4	4.0	1.4×10^6	G 16.4−0.2	9	1.5×10^{49}	3.3×10^5
7(M16)	2.9×10^5	2.0	1.4×10^6	G 17.0+0.8	103	4.3×10^{49}	6.9×10^5

H II regions with temperature of 7000 K. Finally, the total luminosity of the source is estimated from N_L using the calculations by Panagia (1973). This estimate assumes a single zero-age main-sequence (ZAMS) star and hence represents a lower limit to the total luminosity.

Comparison of the luminosities presented in columns (4) and (8) shows that the sources are diverse. For one group (sources 1, 3, 4, 5, and 7), the two luminosity estimates agree to within about a factor of 2, with the far-infrared determinations being consistently higher. This would be expected if each source were in fact powered by a group of stars each of later type than the assumed single star in Table 2.

For sources 2 and 6, however, there are larger discrepancies of the order of a factor of 6 in the two luminosity estimates. In comparison to the first group of sources, these have similar far-infrared and submillimeter emission but much reduced radio continuum emission. A possible explanation is that each of these sources represents a very young OB cluster with reduced radio emission due to optically thick components. The data of Altenhoff *et al.* (1970) do not show optically thick spectra, however. Furthermore, while the 2'.6 radio survey by Altenhoff *et al.* (1978) shows that the radio emission for each is due to relatively weak, small sources, there is little evidence for ultracompact H II regions which would imply very recent star formation. Ultracompact H II regions have, however, been observed in other sources, in particular, source 1, W33 (Haschick and Ho 1983; see also Ho and Haschick 1981).

A more likely explanation is that these two sources represent clusters with optically thin H II regions whose highest mass star is a relatively late O star (e.g., O6.5 or later), whereas each source of the first group is probably a cluster powered by a somewhat earlier type O star (Ho and Haschick 1981).

IV. CONCLUSIONS

1. In the large-beam surveys the galactic ridge appears as separate from discrete sources, although the ridge may itself be a collection of unresolved sources.
2. The discrete sources and the galactic ridge have typical dust temperatures of about 25 K.
3. Within the sources and the ridge, a range in temperatures is required, although we have not modeled the temperature structure.
4. There is a very strong association of far-infrared and thermal radio continuum sources.
5. There is a strong association of far-infrared sources and molecular clouds, but there are molecular clouds which are not far-infrared sources.
6. The galactic ridge component and most of the sources in this region may be associated with the "5 kpc" molecular ring.
7. The large-beam survey detects diffuse emission from evolved H II regions not detected in the JSF small-beam survey. For the evolved sources, the diffuse emission may be energetically comparable or larger than the compact components.
8. There is a significant range in the ratios of infrared to total luminosity as estimated from the radio continuum among the sources. This dispersion may be accounted for by the specific spectral type (e.g., ~05–07) of the most massive star in the presumed O-B cluster.

It is a pleasure to acknowledge the flight operation support of the National Scientific Balloon Facility on flights 1159P for SO and 1209P for GSFC. D. W. Niles gratefully acknowledges support from Colby College.

REFERENCES

Allen, C. W. 1973, *Astrophysical Quantities* (London: Athlone), p. 251.
Altenhoff, W. J., Downes, D., Goad, L., Maxwell, A., and Rinehart, R. 1970, *Astr. Ap. Suppl.*, **1**, 319.
Altenhoff, W. J., Downes, D., Pauls, T., and Schraml, J. 1978, *Astr. Ap. Suppl.*, **35**, 23.
Campbell, M. F. 1979, *Instrumentation in Astronomy III*, *Proc. SPIE.*, **172**, 152.
Campbell, M. F., Hoffmann, W. F., and Thronson, H. A., Jr. 1981, *Ap. J.*, **247**, 530.
Campbell, M. F., Hoffman, W. F., Thronson, H. A., Jr., and Harvey, P. M. 1980, *Ap. J.*, **238**, 122.
Drapatz, S. 1981, in *IAU Symposium 96, Infrared Astronomy*, ed. C. G. Wynn-Williams and D. P. Cruikshank (Dordrecht: Reidel), p. 261.
Elmegreen, B. G., Lada, C. J., and Dickenson, D. F. 1979, *Ap. J.*, **230**, 415.
Gispert, R., Puget, J. L., and Serra, G. 1982, *Astr. Ap.*, **106**, 293.
Gordon, M. A., and Burton, W. B. 1976, *Ap. J.*, **208**, 346.
Harvey, P. M., Campbell, M. F., and Hoffmann, W. F. 1977, *Ap. J.*, **211**, 786.
Haschick, A. D., and Ho, P. T. P. 1983, *Ap. J.*, **267**, 638.
Ho, P. T. P., and Haschick, A. D. 1981, *Ap. J.*, **248**, 622.
Hoffmann, W. F., Frederick, C. L., and Emery, R. S. 1971, *Ap. J.* (*Letters*), **170**, L89.
Jaffe, D. T., Stier, M. T., and Fazio, G. G. 1982, *Ap. J.*, **252**, 601 (JSF).
Keene, J. 1981, *Ap. J.*, **245**, 115.
McBreen, B., Fazio, G. G., and Jaffe, D. T. 1982, *Ap. J.*, **254**, 126.
Nishimura, T., Low, F. J., and Kurtz, R. F. 1980, *Ap. J.* (*Letters*), **239**, L101.
Okuda, H. 1981, in *IAU Symposium 96, Infrared Astronomy*, ed. C. G. Wynn-Williams and D. P. Cruikshank (Dordrecht: Reidel), p. 247.
Olthof, H. 1974, *Astr. Ap.*, **33**, 471.
Panagia, N. 1973, *A.J.*, **78**, 929.
Rubin, A. H. 1968, *Ap. J.*, **154**, 391.
Schwartz, P. R. 1982, *Ap. J.*, **252**, 589.
Scoville, N. J., and Kwan, J. 1976, *Ap. J.*, **206**, 718.
Silverberg, R. F., Hauser, M. G., Mather, J. C., Gezari, D. Y., and Kelsall, T. 1979, *Instrumentation in Astronomy III*, *Proc. SPIE*, **172**, p. 149.
Stier, M. T., Jaffe, D. J., Fazio, G. G., Roberge, W. G., Thum, C., and Wilson, T. L. 1982, *Ap. J. Suppl.*, **48**, 127.
Thaddeus, P. 1982, private communication.
Thronson, H. A., Jr., and Harper, D. A. 1979, *Ap. J.*, **230**, 133.
Ward, D. B., Gull, G. E., and Harwit, M. 1977, *Ap. J.* (*Letters*), **214**, L63.
Wilson, T. L., Fazio, G. G., Jaffe, D., Kleinmann, D., Wright, E. L., and Low, F. J. 1979, *Astr. Ap.*, **76**, 86.

M. F. CAMPBELL: Department of Physics and Astronomy, Colby College, Waterville, ME 04901

M. G. HAUSER, T. KELSALL, and R. F. SILVERBERG: Laboratory for Extraterrestrial Physics, NASA/Goddard Space Flight Center, Code 693.2, Greenbelt, MD 20771

W. F. HOFFMANN: Steward Observatory, University of Arizona, Tucson, AZ 85721

D. W. NILES: Physics Department, University of Wisconsin, Madison, WI 53706

M. T. STIER: Perkin Elmer Corporation, Space Sciences Division, M/S 897, 100 Wooster Heights Road, Danbury, CT 06810

H. A. THRONSON, JR: Department of Physics and Astronomy, University of Wyoming, University Station, Box 3905, Laramie, WY 82071